

Electronic Supplementary Information

Nitrogen-doped sp^3 carbon dots catalyse two-electron electrochemical oxygen reduction for efficient production of hydrogen peroxide

*Jianhua Shen, Xinyue Qiu, Yihua Zhu**

Key Laboratory for Ultrafine Materials of Ministry of Education, Shanghai Engineering Research Center of Hierarchical Nanomaterials, Frontiers Science Center for Materiobiology and Dynamic Chemistry, School of Materials Science and Engineering, East China University of Science & Technology, Shanghai 200237, China

E-mails: Yihua Zhu (yhzhu@ecust.edu.cn)

S1. Experimental Parameters Information

Electrochemical measurements

For the three-electrode system used for electrochemical testing, the working electrode consisted of a glassy carbon disk electrode and a platinum ring electrode (glassy carbon disk electrode outer diameter: 5.61 mm, platinum ring outer diameter: 7.92 mm, platinum ring inner diameter: 6.25 mm). Ag/AgCl electrode and platinum wire electrode were used as reference electrode and counter electrode, respectively. 2 mg catalyst was added to 500 μL deionized water, 475 μL ethanol, and 25 μL 0.5 wt.% Nafion solution and ultrasonically dispersed for 30 min to obtain a homogeneous catalyst ink. The experimental pretreatment step of the working electrode was to polish the surface of the glassy carbon electrode using Al_2O_3 powder of different particle sizes in combination with ultrasonic surface cleaning. Afterwards, 10 μL of ink was added to the surface of the glassy carbon disk electrode and air dried. The catalyst loading was about 80 $\mu\text{g cm}^{-2}$.

Subsequently, electrochemical tests were performed under a range of conditions.

The catalysts were activated by cyclic voltammetry (CV) until the CV curve was completely stabilized before formal testing.

The linear sweep voltammetry (LSV) curve was tested at a potential interval of 0-1 V vs. RHE with a constant voltage of 1.2 V vs. RHE applied continuously to the ring electrode. To correct the polarization curve, the background current measured in the N_2 -saturated electrolyte was subtracted.

All electrochemical measurements were conducted in 0.1 M N_2/O_2 saturated KOH solution (pH=13), and the reversible hydrogen electrode (RHE) was used as the reference for all potentials in this work. They were calculated by equation (S-1).

$$E_{\text{RHE}} = E_{\text{Ag/AgCl}} + 0.197 + 0.0591 \cdot \text{pH} \quad (\text{S-1})$$

The hydrogen peroxide selectivity ($\text{H}_2\text{O}_2\%$) and the number of transferred electrons (n) of DCDs were quantitatively characterized by the formula (S-2) - (S-3):

$$\text{H}_2\text{O}_2(\%) = 200 \times \frac{\frac{I_r}{N}}{I_d + \frac{I_r}{N}} \quad (\text{S-2})$$

$$n = \frac{4 I_d}{I_d + \frac{I_r}{N}} \quad (\text{S-3})$$

Where, separately, I_d and I_r stand for disk and ring currents. N represents RRDE's current collection efficiency, which is calibrated to 0.37.

The corresponding electrochemical active surface area (ECSA) can be calculated from formula (S-4):

$$ECSA = \frac{C_{dl}}{A \times C_s} \quad (S-4)$$

Where A is the catalyst loading on the surface of the disk electrode, and $C_s = 40$ mF cm⁻², which is the empirical constant for the capacitance value per unit area.

Characterizations

Using an X-ray diffraction spectrometer (XRD), model Rigaku D/MAX 2550, with a scanning range of 10-90° and a sweep speed of 4° min⁻¹, the material phase structure of the materials was analysed. The surface morphology of the material was investigated by transmission electron microscopy (TEM). The instrument of choice was a Talos F200X field emission transmission electron microscope with a 200 kV operating voltage. Raman spectroscopy was used to analyse the carbon material for defect information and sp^2/sp^3 conformation. A Renishaw Inquiry Reflex device was utilized, with wave number settings of 500-3500 cm⁻¹ and an excitation wavelength of 325 nm. Fourier transform infrared (FTIR) spectroscopy with a Thermo Fisher Nicolet iS50 equipment was used to examine the surface functional groups of the materials. Thermo Fisher ESCALAB 250Xi was utilized to conduct the X-ray photoelectron spectroscopy (XPS) analysis of surface chemistry. All data were charge adjusted using a C 1s peak at 284.8 eV.

Cerium sulphate titration method

By Cerium sulphate titration method, the concentration of H₂O₂ generated by the oxygen reduction reaction catalysed by N-DCDs under CA testing was determined. The equation of Ce(SO₄)₂ reacting with H₂O₂ in aqueous solution is as follows:



When H₂O₂ is added, the yellow Ce⁴⁺ solution becomes a transparent Ce³⁺ solution. The concentration of H₂O₂ in the electrolyte can be determined by analysing the absorbance at 317 nm using UV-vis spectroscopy, which is to measure the concentration of Ce⁴⁺. The 0.1 mol L⁻¹ standard cerium sulphate solution was diluted to a concentration gradient of 0.1 - 0.5 mM Ce(SO₄)₂ solution and measured using UV-vis absorption spectroscopy.

Subsequently, an appropriate amount (50 μL) of the electrolyte solution replaced every hour of the chronoamperometry test was extracted and added to 3 mL of 0.4 mmol L^{-1} cerium sulphate solution, mixed well and then subjected to UV-vis test. The H_2O_2 yield can be assessed from this.

The Faraday efficiency of H_2O_2 is calculated as follows:

$$\text{Faradaic Efficiency (\%)} = \frac{2 CFV}{Q} \quad (\text{S-6})$$

In the formula, C is the actual concentration of H_2O_2 (mol L^{-1}), F is the Faraday constant (96485 C mol^{-1}), V is the volume (L), and Q is the number of transferred charges (C) obtained by integrating the I-t curve.

Computational Details

All the DFT calculations were conducted using the Dmol3 module of Materials Studios 2017. The electronic exchange and related energy were treated using the Perdew, Burke and Ernzerhof (PBE) functional within the generalized gradient approximation (GGA). The conductor like screening model (COSMO) method was adopted to consider the electrostatic interaction of adsorbate and water solvent. The DFT semi-core pseudo potentials (DSPPs) core treatment with the relativistic effects were implemented to consider the core-electron (e^-) interaction, which superseded core e^- by a single valid electric potential to simplify the calculations. The numerical basis set of double numerical plus polarization (DNP) was utilized. Thermal smearing of orbital occupation is set to 0.005 Ha (1 Ha = 27.21 eV). A $3 \times 3 \times 1$ Monkhorst-Pack grid of special k-points was used for Brillouin zone integration. The SCF density convergence tolerance was 1×10^{-5} Ha. The maximum force, displacement, and energy of geometry optimal convergence tolerance are 0.004 Ha/ \AA , 0.005 \AA , and 2×10^{-5} Ha. The standard hydrogen electrode (SHE) model was calculated the Gibbs free energy change (ΔG) for each basic step. Based on this method, the ΔG value can be determined as follows:

$$\Delta G = \Delta E + \Delta ZPE - T\Delta S + \int C_p dT \quad (\text{S-7})$$

where ΔE is the electronic energy difference calculated from DFT, ΔZPE is the change in zero-point energies, T is the ambient temperature, C_p is the heat capacity and ΔS is

the entropy change. The thermodynamic properties of gas-phase molecules and ZPE contribution of adsorbed species are obtained through vibrational frequencies. The computational hydrogen electrode (CHE) model was utilized to specify the Gibbs free energy of the proton-electron pair as the function of electrical potential.

Free energy is calculated as:

$$F = E + \mu_e * n_e \quad (\text{S-8})$$

Where E is the total energy of the system, μ denotes the chemical potential of electrons at a given potential, and n_e represents the net charge of the system at $U_{\text{RHE}} = 0.7 \text{ V}$.

The DCD (111) and (110) surfaces were modelled by periodically repeated four-layer slabs with (3×3) unit cells. The Brillouin zone was sampled with the Monkhorst-Pack scheme and $3 \times 3 \times 1$ k-point mesh. The atoms in the top one layer was fully relaxed, while the rest of the atoms were fixed in their equilibrium positions. One vacuum slab of 20 \AA was added in the z direction to avoid periodic interactions.

S2. Figures and tables

Table S1. Elemental contents obtained by XPS.

Samples	C content /at.%	O content /at.%	N content /at.%
DCDs	63.24	36.76	/
N-DCDs	76.38	18.73	4.89

Table S2. Functional group contents obtained by XPS C 1s.

Samples	sp^3 content /at.%	sp^2 content /at.%	C-O/C-N content /at.%	C=O content /at.%
DCDs	56.07	20.40	21.70	1.83
N-DCDs	69.56	3.61	15.35	11.48

Table S3. Functional group contents obtained by XPS O 1s.

Samples	C-O content /at. %	C=O content /at. %	N-O content /at. %
DCDs	94.37	5.63	/
N-DCDs	55.63	39.51	4.86

Table S4. Functional group contents obtained by XPS N 1s.

Sample	N- <i>sp</i> ³ C content /at. %	N- <i>sp</i> ² C content /at. %	N-O content /at. %
N-DCDs	51.13	27.40	21.47

Table S5. H₂O₂ selectivity compared with previous works in 0.1M KOH electrolyte.

Catalysts	Onset Potential (V vs. RHE)	H ₂ O ₂ Selectivity (%)	Productivity	Faradaic Efficiency (%)	Ref.	Ref. Number
N-DCDs	0.72	99.0	613.58 mmol g _{Catalyst} ⁻¹ h ⁻¹	90.4	This work.	/
B-C	0.77	85.0	7.36 mmol h ⁻¹ cm ⁻²	87	<i>Nat. Commun.</i> , 2021, 12 , 4225.	Ref. 7
CB+CTAB	0.80	95.2	/	/	<i>Chem</i> , 2020, 6 , 1443-1458.	Ref. 15
HCNFs	0.75	97.3	6.37 mmol L ⁻¹ h ⁻¹	/	<i>Angew. Chem., Int.</i> <i>Ed. Engl.</i> , 2021, 60 , 10583-10587.	Ref. 16
O-CNTs	0.80	90.0	/	/	<i>Nat. Catal.</i> , 2018, 1 , 156-162.	Ref. 42
N-CBMC- 500	0.74	95.9	2.11 mol g _{Catalyst} ⁻¹ h ⁻¹	69.3	<i>J. Mater. Chem. A</i> , 2022, 10 , 4749- 4757.	Ref. 35

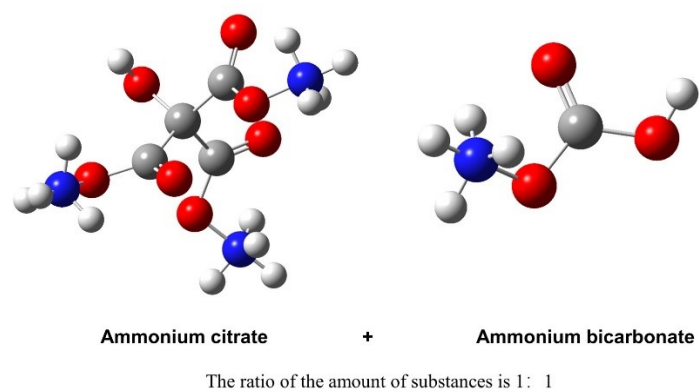


Fig. S1 Precursor formulation structure and preparation scheme for N-DCDs.

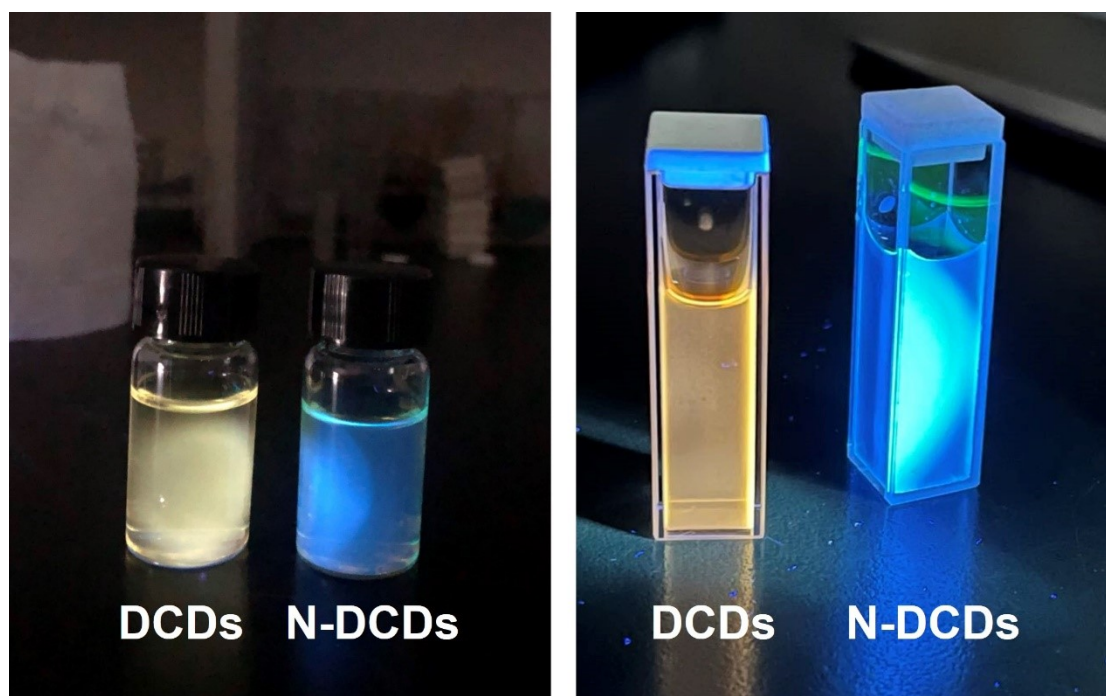


Fig. S2 Aqueous solutions of DCDs samples emit fluorescence in different wavelengths.

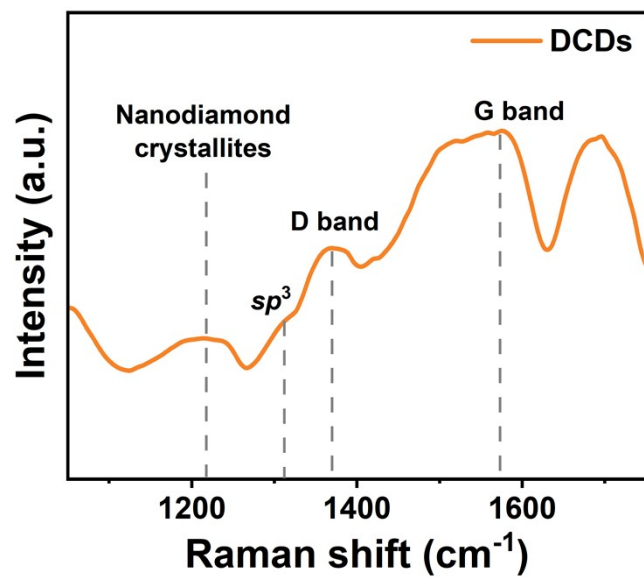


Fig. S3 Raman spectrum of DCDs.

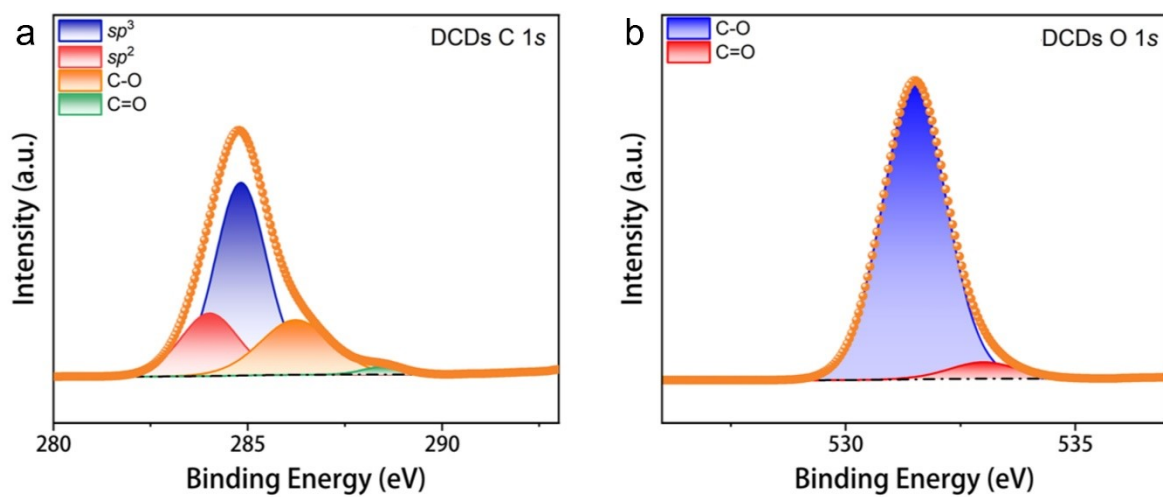


Fig. S4 High-resolution XPS spectra of (a) C 1s and (b) O 1s of DCDs.

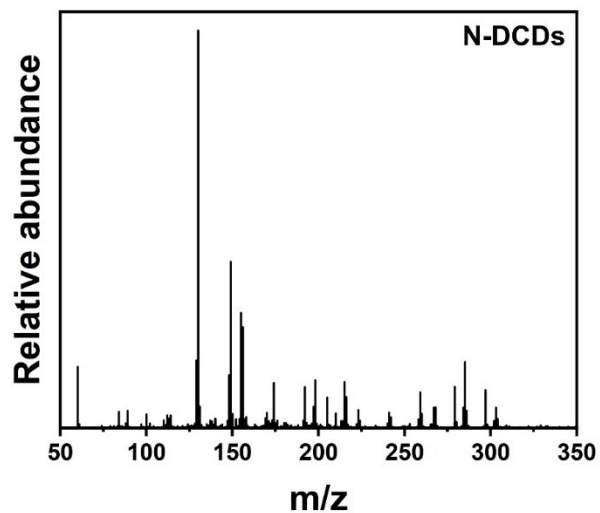


Fig. S5 Mass spectrum of N-DCDs.

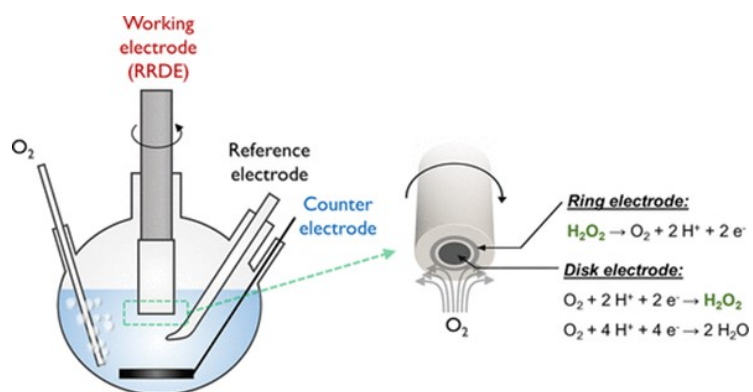


Fig. S6 RRDE device schematic. (Ref. 45)

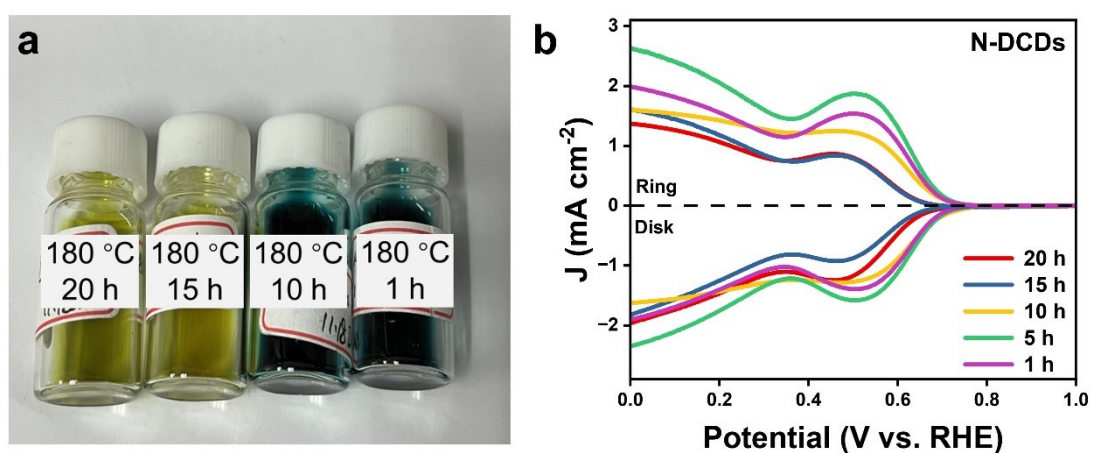


Fig. S7 (a) Sample colors and (b) LSV curves of several N-DCDs prepared at different hydrothermal times at constant temperature.

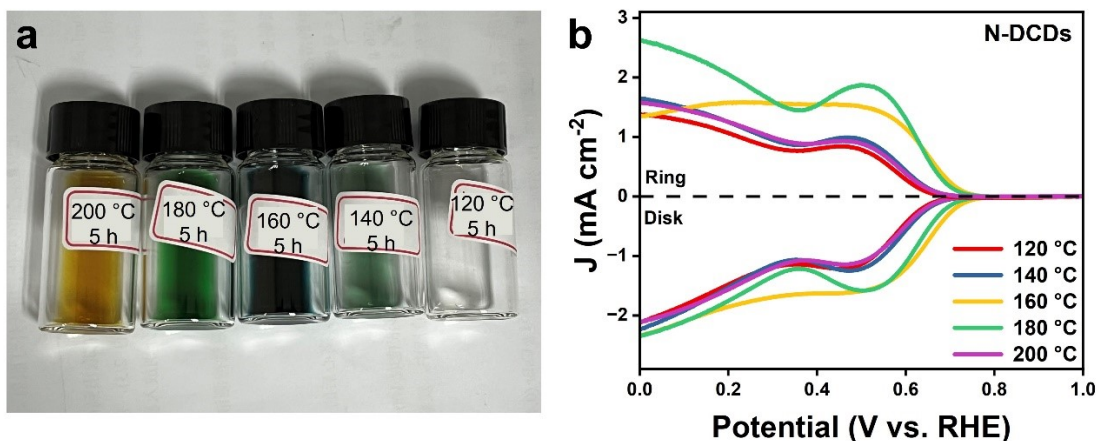


Fig. S8 (a) Sample colors and (b) LSV curves of several N-DCDs prepared at different hydrothermal temperatures at constant time.

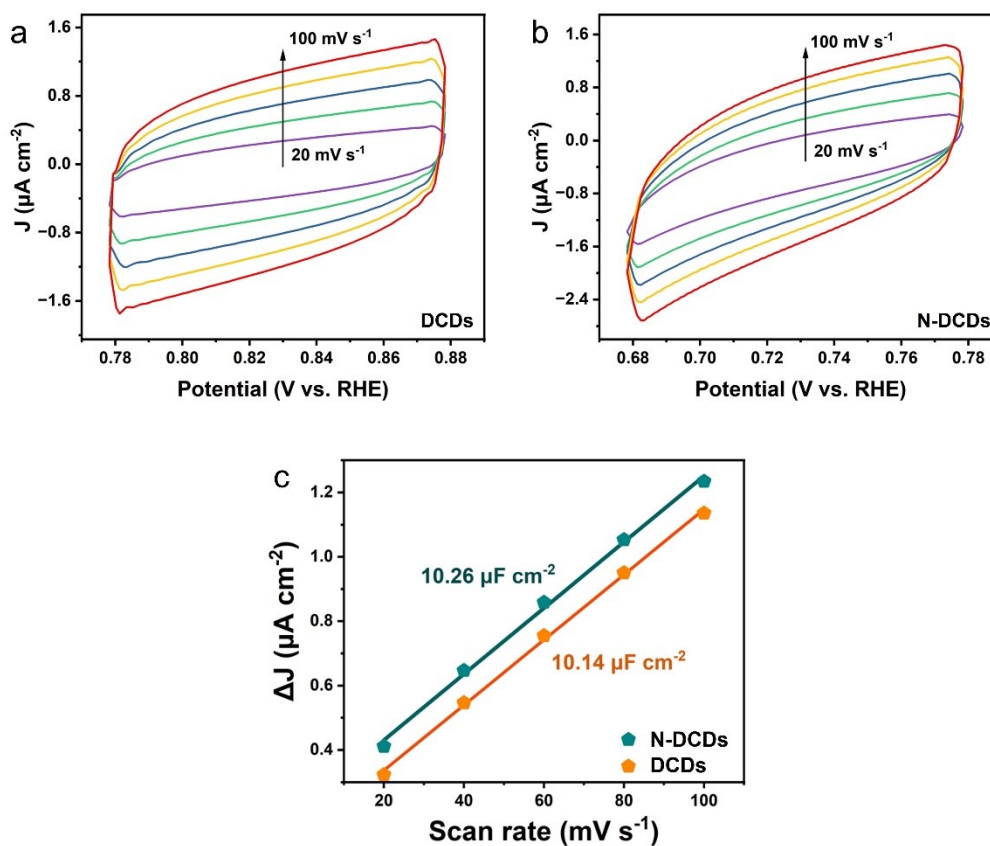


Fig. S9 CV curves of (a) DCDs and (b) N-DCDs at different scanning rates acquired in N_2 -saturated 0.1 M KOH solution, which were used to calculate C_{dl} and ESCA; (c) Electrochemical double-layer capacitances (C_{dl}) fitted from the CV curves at different scanning rates.

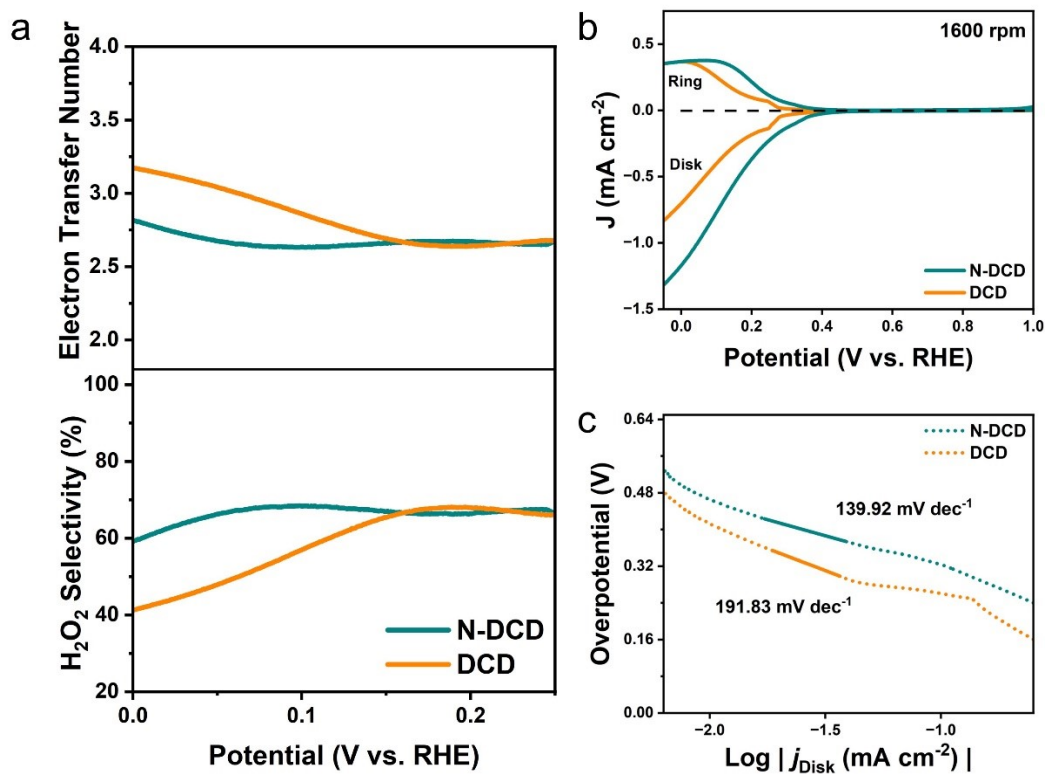


Fig. S10 In O_2 -saturated 0.1 M Na_2SO_4 electrolyte: (a) H_2O_2 selectivity and electron transfer number derived from polarization curves, (b) RRDE polarization curves obtained at 1600 rpm, (c) Tafel slope derived from disc current density.

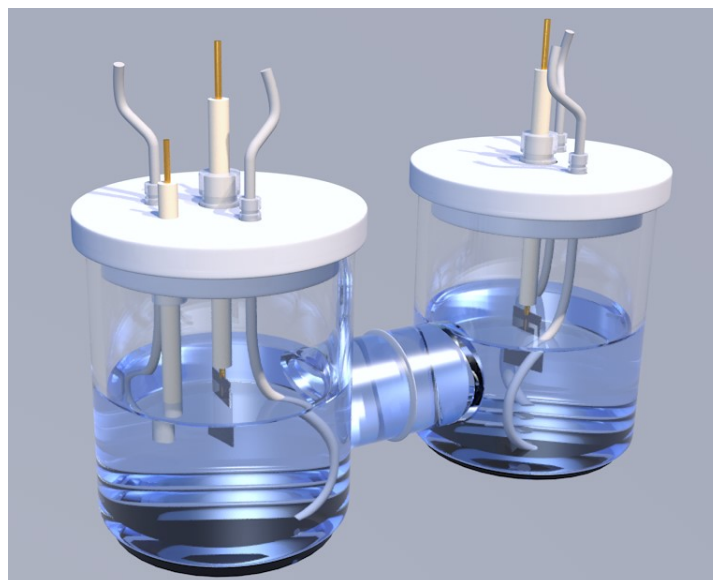


Fig. S11 Assembled H-type electrolytic cell model.

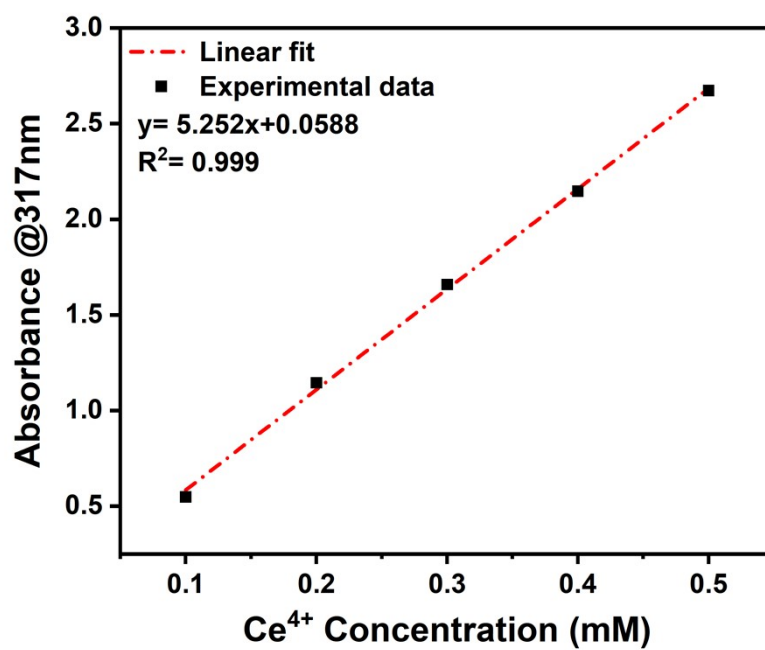


Fig. S12 The standard concentration curve of Ce(SO₄)₂ solution.

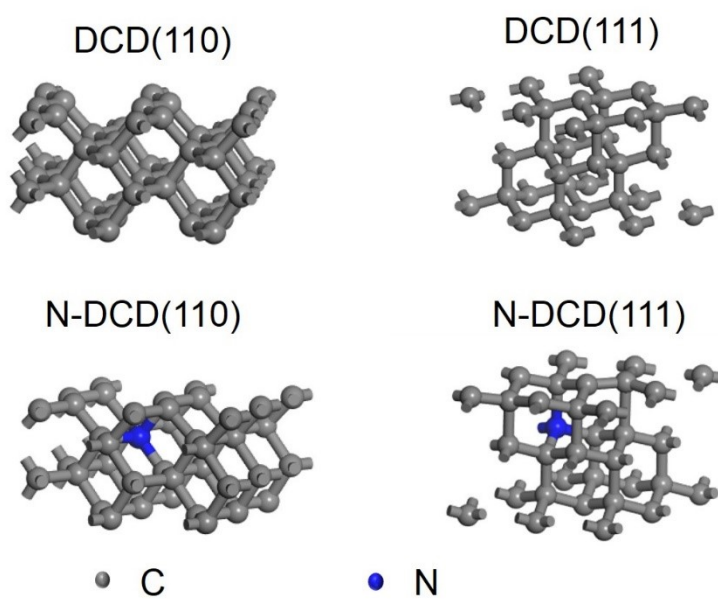


Fig. S13 Computational models of DCD (110), DCD (111), N-DCD (110), and N-DCD (111).

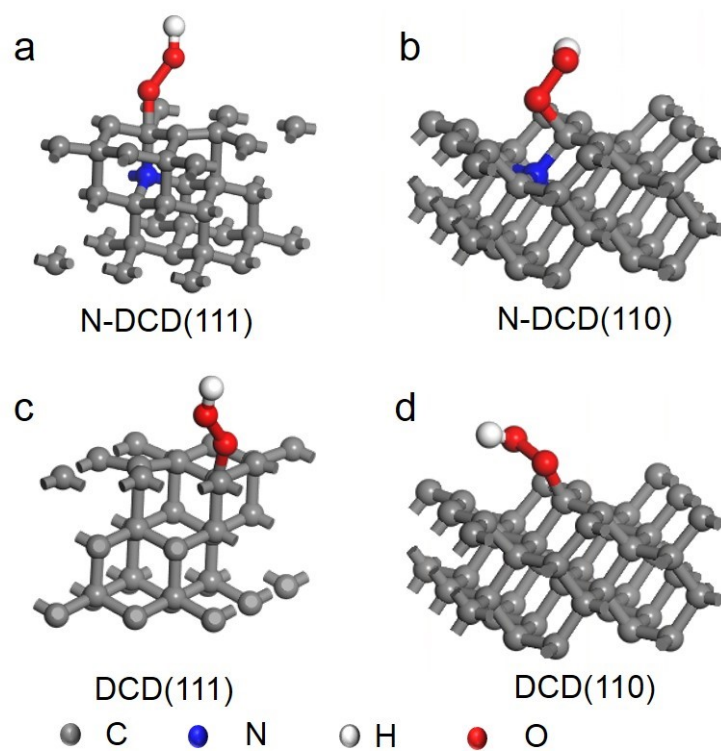


Fig. S14 Computational models of (a) N-DCD(111), (b) N-DCD(110), (c) DCD(111), and (d) DCD(110); where the blue atoms represent the doped nitrogen, and *OOH intermediate adsorbed at different sites.